Investigation of the Influence Factors on Distortion in Induction-Hardened Steel Shafts Manufactured from Cold-Drawn Rod

JUAN DONG, JEREMY EPP, ALEXANDRE DA SILVA ROCHA, RAFAEL MENEZES NUNES, and HANS WERNER ZOCH

In this study, the distortion of steel shafts was investigated before and after induction hardening. Several essential influencing factors in the manufacturing process chain regarding cold drawing, cutting method, notches on the shafts, and induction hardening were analyzed by design of experiment (DoE). Further necessary examinations of microstructures, hardness profile, segregation of chemical composition, and residual stress state were conducted for understanding the distortion behavior. The results of the statistical analysis of the DoE showed that the drawing process is the most important factor influencing distortion. The surface hardening depth of induction hardening is the second main factor. The relationship between inhomogeneities in the work pieces and the distortion was finally discussed.

DOI: 10.1007/s11661-015-3250-4

I. INTRODUCTION

COILED steel wires are frequently taken as semi-finished materials to produce machine components, for example automotive shafts. A typical manufacturing process can consist of uncoiling, pre-straitening, cold forming, fine cross-roll straightening, machining as well as heat treatment processes.[1,2] The heat treatment at the end of the manufacturing cycle is generally used to enhance the material properties. However, in nearly all cases, the heat treatment also leads to an undesirable change in dimensions and shapes, *i.e.*, "distortion," of the component. If the alterations exceed the tolerances, an additional corrective operation, such as straightening and/or final grinding, has to be carried out, high costs occur.[1] Nowadays, it is well-known that the heat treatment is not the only reason for causing the distortion of components, but it can release the distortion potential, which has been accumulated in the components during a manufacturing process, which constituted the series of operations.[2]

Cold forming processes are used increasingly in the industry production because of its energy efficiency, cleanness, no loss of material in the form of chips, improvement of dimensional accuracy, and surface finish. Cold forming is defined as a forming process or plastic deformation operation carried out at temperatures below the recrystallization temperature of the workpiece material, but more often it is simply referred to as the forming process at room or ambient temperature.[3] Cold drawing is counted among the most commonly used cold forming operations. Large quantities of metal or alloy products such as rods, tubes, and wires with various special sections can be produced by cold drawing process. Bars are frequently given a light sizing pass, reducing the diameter slightly to improve surface finish, and dimensional tolerance. The plastic deformation in cold drawing is not uniform, causing inhomogeneous hardness distribution and residual stresses. This depends essentially on the die angle used in the process and is more pronounced for higher angles.[3]

The changes in the material's properties by one process step can influence the following manufacturing step. Particularly, if cold-formed components need to be heat treated (hardened) a broad range of distortions can occur.[4,5] It has been demonstrated that the distortion of components is connected to many factors in the whole manufacturing process. These factors can be the components' geometry; the chemical composition and local variations; the microstructures; the mechanical history of the components; the generation and relaxation of stresses/residual stresses as well as the local time–temperature sequences; and phase transformations at elevated temperature.[6,7] In order to control distortion in such products, the whole manufacturing chain has to be analyzed.

In the current study, an analysis of the whole manufacturing process chain for the production of steel shafts from cold-drawn rods was carried out with a statistical approach using the "design of experiments (DoE)."[8–10] The factors considered in the DoE were the

JUAN DONG, Research Engineer, JEREMY EPP, Research Group Leader, and HANS WERNER ZOCH, Professor and Director, are with the Division of Materials Science, Foundation Institute for Materials Science, Badgasteiner Str. 3, 28359 Bremen, Germany. Contact e-mail: dong@iwt-bremen.de ALEXANDRE DA SILVA ROCHA, Professor, is with the PPGEM, Metal Forming Laboratory, Universidade Federal do Rio Grande do Sul, Porto Alegre, Brazil. RAFAEL MENEZES NUNES, Postdoctoral Researcher, is with the LAMEF, Physical Metallurgy Laboratory, Federal University of Rio Grande do Sul, Porto Alegre, Brazil.

Manuscript submitted July 7, 2015.
Article published online November 25, 2015

geometry of the cold drawing tool, the method for cutting the bars, the geometry of the shafts by machining the work pieces with notches, and the induction hardening depth. The shafts were characterized after several main process steps in terms of microstructure, hardness, residual stresses, and local chemical composition in order to clarify the influence of the significant factors on distortion.

II. EXPERIMENTAL DETAILS

The investigated sample material was an AISI 1045 steel. The semi-finished material was produced by continuous casting, hot rolling, and coiling. The chemical composition analyzed by Optical Emission Spectroscopy (OES) is given in Table I. It is within the reference range of the standard steel grade AISI 1045.

The investigated manufacturing process chain (Figure 1) starts with the coiled wire. The initial mean diameter of the wire is 21.49 ± 0.03 mm with variations between 21.31 and 21.59 mm. The wire is uncoiled, pre-straightened horizontally and vertically, shot blasted, and cold drawn to the targeted diameter of 20.25 mm. For cold drawing, two different die angles were tested. After cold drawing, the wire was shear cut into 6 meter bars. A cross-roll straightening (CRS), with two crossed rolls at an angle of 16 deg, was applied to the 6 meter bars. From these bars, the samples were cut by saw or shear to a length of 410 mm. The samples were machined to reach 400 mm in length, with two notches of 16 and 18 mm in diameter (see Figures 3 and 4). Central holes were further machined at each end of the samples for fixing them during induction hardening. The induction hardening treatments were performed to obtain a target Surface Hardening Depth (SHD) of either 1.2 mm or 2.2 mm followed by a tempering treatment at 443 K (170 °C) for 2 hours. The shafts were finally ground to the designed size and shape.

The variation of the cold drawing process was achieved by using two new dies with different drawing angles of 15 or 20 deg ($\alpha = 7.5$ or 10 deg), respectively (Figure 2). Deformation zone geometry for wire drawing, can be characterized by a single parameter, Δ, defined as the ratio of the mean thickness, $h = (D_0 - D)/2$, of the work metal to the contact length, $L = (D_0 - D)/(2\sin\alpha)$, between tool and work metal. The parameter Δ increases with increasing drawing die angle.[3] From the reduction in diameter (as mentioned above) a mean area (cross section) reduction of 11 pct ($\Delta A/A_0$) and a length increase of 12 pct ($\Delta L/L_0$) are resulted assuming that the volume is constant. The angular position of the bars was marked with "0 deg" related to the top position of the drawing die. The other angular positions were defined after "right-hand rule": the right thumb pointed the drawing direction. The guide marks of "0 deg" and drawing direction were used for all samples and were kept through the whole process chain in order to serve as reference for all analyses. The longitudinal lines at the surface of different angular positions are defined as "angle-lines" *e.g.*, 0 deg line, 45 deg line, *etc.* The diameters connected two angular positions at a cross section are named as "diameter-lines" *e.g.*, 0 to 180 deg line, 90 to 270 deg line *etc.*

Table I. Chemical Composition of the Used Steel Grade, Balance Fe

Element	C	Si	Mn	P	S	Cr	Mo	Ni	Cu	Nb
Mass pct	0.47	0.23	0.87	0.024	0.034	0.09	0.02	0.08	0.16	0.02

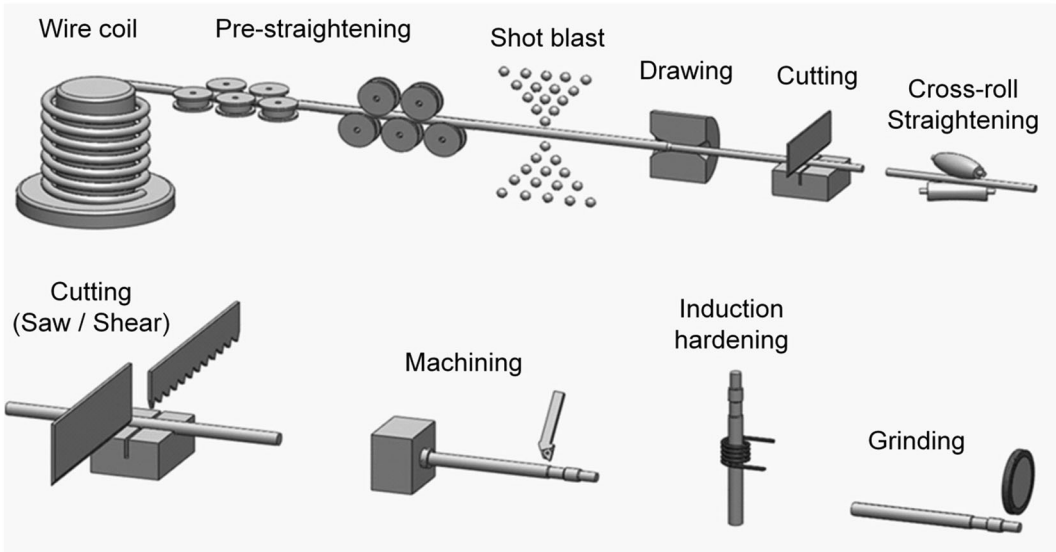

Fig. 1—Schematic illustration of the manufacturing process chain.

A multi-frequency induction hardening equipment (type SINAC 200/300 FMC EFD, Freiburg, Germany) was used to carry out the induction heat treatments (Figure 3(a)). The samples with central holes at top and bottom were clamped between two tips and rotated at 500 min^{-1}. The inductor of 22 mm in diameter was initially placed at the bottom and moved upwards with a feed rate of 900 mm/minutes. A mid-frequency of 12.1 kHz was used and the power was varied to obtain the desired SHD. The quenching nozzles were placed underneath the inductor and the quenchant was 12 mass pct aquatenside®, with a flow rate of 40 L/minutes. A uniform SHD over the length of the notched shafts could be achieved by several preliminary tests for determining the adequate parameters for the varied diameters. The heating power was 104 to 110 and 126 to 136 kW, resulting in austenitizing temperatures of about 1123 K and 1243 K (850 °C and 970 °C) for SHD 1.2 and 2.2 mm, respectively. The SHD was determined at 80 pct of the minimum required hardness (600HV1) on the hardness profiles in the radial direction.

Three-dimensional coordinate measurements were performed in order to determine the shape and sizes of the samples after the different process steps using a Coordinate measuring machine (Leitz PMM 654). The accuracy of the measurement was 1.2 μm. The setup of the measurement is shown in Figure 3(b). The samples were clamped at two points on the plate of the equipment with the 0 deg mark always at the top position. 20 circles and 360 points for each circle were measured to define the shape and size of the bars. The 20 circles were located at pre-defined distances (Z = 2, …, 398 mm) from the notched end of the samples (Figure 4). The evaluation of the data was performed by using excel macros. Each circle was fitted with a best fit circle by a least squares method and the center positions of the circles were then calculated. Details of the method can be found in Reference 11. The projection of these centers on x–y planes in the axial (z) center of each sample creates a vector. The vector length is an expression for the curvature and its orientation in the x–y plane the expression of the orientation of this curvature. It should be mentioned that the long thin shaft was not measured by holding it between center holes, in order to avoid the influence of the force, which has to be used for the sensor to touch the shaft, on the results.

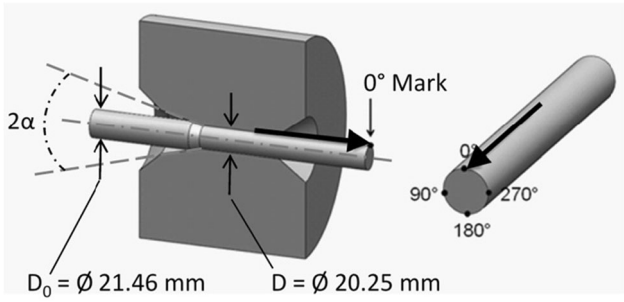

Fig. 2—Schematic illustration of the drawing process, drawing die, and the marked angle positions.

Residual stresses were analyzed by X-ray diffraction (XRD) using the conventional $\sin^2\psi$-method.[12,13] A diffractometer (GE Inspection Technologies, Type MZ VI) with Vanadium filtered Cr-Kα-radiation was employed. A primary beam aperture of 2 mm diameter and a scintillation counter with a 2-mm secondary slit for detecting the diffracted beam were used for the local analysis along the length and around the periphery of the drawn cylinders. The {211} diffraction peak of α-iron was measured.[12,13] The Full Width at Half Maximum (FWHM) values of the diffraction peaks are also evaluated, which give further information about microstresses and crystallite size in the microstructure. The AISI 1045 steel contains about 6.7 vol pct of cementite (Fe_3C) in initial heat treatment condition. A contribution of cementite on the macroscopic residual stress state is present,[14,15] this was, however, for simplification not considered in the present work. The residual stresses were mainly measured in axial direction as the distortion of the samples mainly consists of

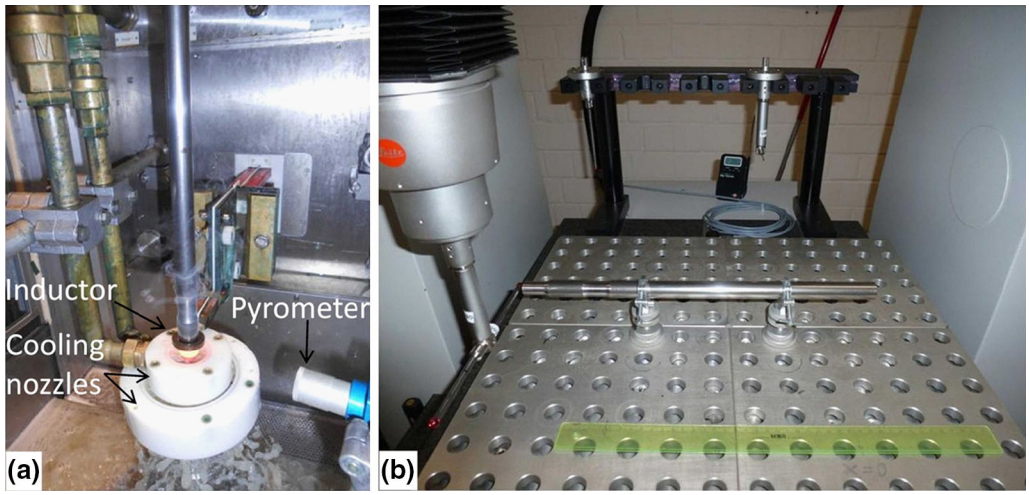

Fig. 3—Setup for induction hardening (*a*); Setup for 3-dimensional co-ordinate measurements (*b*).

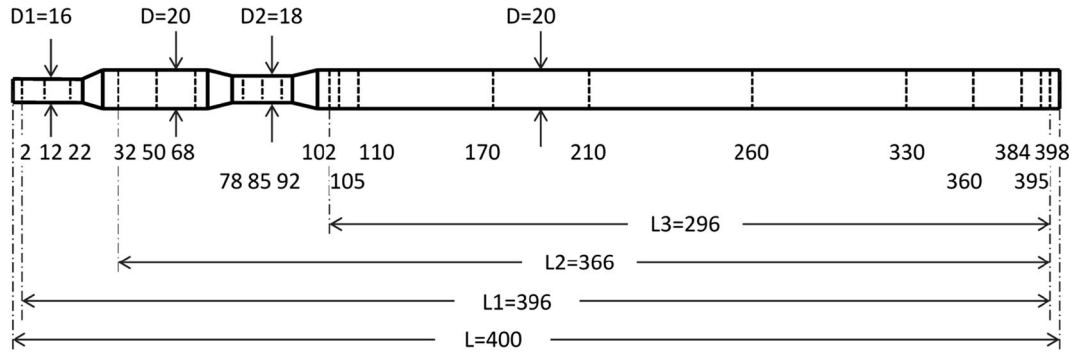

Fig. 4—Schematic illustration of a shaft and the 20 circles (dotted lines) for the 3D measurements (units in mm); *D* the diameter after drawing, *D*1 and *D*2 the diameters of the notches; *L* the length of the sample, *L*1, *L*2, and *L*3 the lengths between the circles used for evaluation).

Table II. Factors and Levels of the Statistical Experiments

Factor Code	A	B	C	D
Factor	drawing angle	cutting method	sample geometry, notch	induction hardening, SHD
Level −	15 deg	saw	yes	1.2 mm
Level +	20 deg	shear	no	2.2 mm

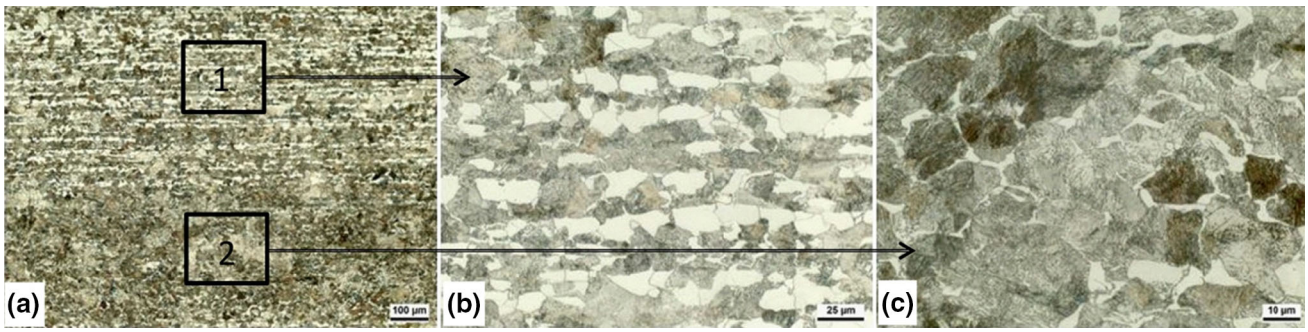

Fig. 5—Microstructure at low magnification (*a*); enlarged microstructure in area 1 (*b*) and enlarged microstructure in area 2 (central segregation) (*c*).

bending. The residual stresses distributed over the cross section of the samples were measured *via* neutron diffraction and were published elsewhere.[16]

For the analysis of the manufacturing process regarding distortion, the experiments were designed by a full factorial DoE plan with 2^4 (=16) experiments.[8–10] Table II gives an overview of the factors and levels considered on the DoE. The amplitude of the curvature after hardening has been used as a response. At least 5 parallel samples for each of the 16 experiments were used for statistical validation of distortion. All 3D measurement data were input to analyze the distortion behavior and the statistical evaluation of the experimental data was carried out by linear regression model with the software Minitab® version 16 (Minitab Ltd, Coventry, UK).

The microstructure of the samples was investigated by optical microscopy. After grinding with silicon carbide paper up to 1200 grit and polishing with 1 micron diamond water lubricant, the samples were etched with 3 mass pct nital (a solution of alcohol and 3 vol pct HNO_3). Hardness profiles were determined along four diameter lines on the cross sections with Vickers hardness tester. The chemical segregations were determined by the Electron Microprobe Analysis (EMPA).

III. RESULTS AND DISCUSSION

A. *Inhomogeneities in the Material*

The local variation of the chemical composition of the material and of the microstructure as carriers of distortion potential was inspected by optical microscopy and EMPA. The microscopic structure of the samples is characterized by alternated pearlite and ferrite bands along the axial direction (Figure 5) due to the previous rolling process, while the amount of pearlite is higher in the central area than in the mid-radius area (Figure 5(c)). This is due to a macrosegregation of alloying/accompanying elements (*e.g.*, Mn, Cr, C, S, P *etc.*) during solidification. This central segregation appears in the macrostructure of the longitudinal section as a dark-etched band presenting variation along the axial direction (Figure 6(a)).

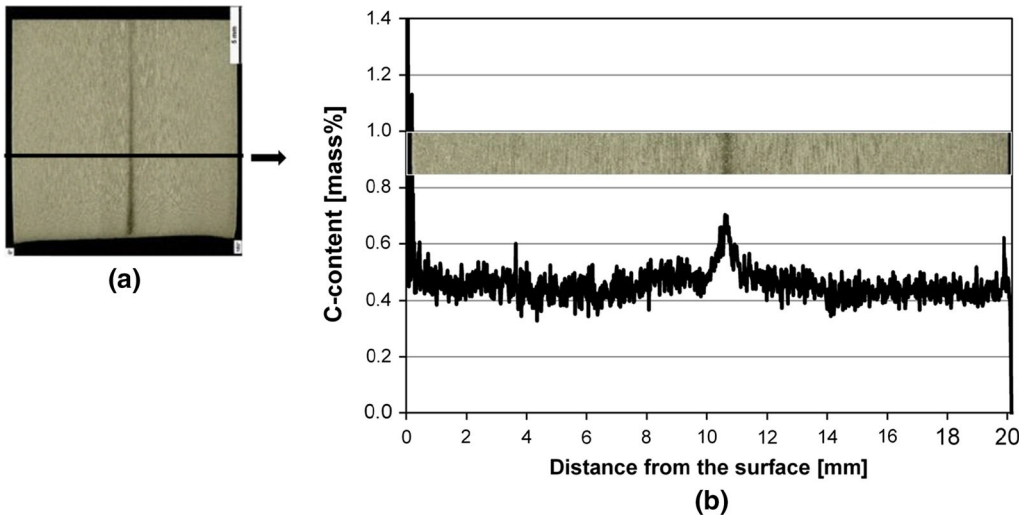

Fig. 6—Macrostructure at a longitudinal section (*a*); (*b*) carbon-content distribution (line) analyzed by EPMA along the diameter with 20 μm width marked with the line in (*a*).

Figure 6(b) shows the local carbon content along the shaft diameter of a sample after drawing (15 deg drawing angle) and cross-roll straightening (CRS). The horizontal image represents the microstructure of the analyzed area with 20 μm in width, in which the carbon concentration was detected from a grid of 1000 points along the diameter and 200 points in width. The average values of the 200 points in width at each distance resulted in the carbon distribution along the diameter presented in Figure 6(b). The mean carbon content is 0.45 $\pm$ 0.05 mass pct. In the segregated central area, the maximum value reached 0.7 mass pct. Similarly, a segregation of manganese was detected. The maximum value reached 1.4 mass pct in the dark area of the microstructure (Figure 6), while the mean manganese content is 0.99 $\pm$ 0.07 mass pct. It can also be observed that the position of the central segregation is eccentric by about 0.6 mm.

The position and the characteristic of the central segregations varied in the longitudinal direction of the rods. It was observed frequently in the microstructures (Figure 13), in which the segregations appear variably in different cross sections in the same sample and in different samples of the same drawing process.

B. *Inhomogeneities Generated by Manufacturing Processes*

The mechanical history of the work piece as another distortion potential could be analyzed in the samples which passed the cold drawing, CRS, cutting, and machining processes. As a consequence of inhomogeneous plastic deformation in the forming processes, cold working leading to an increasing hardness can be investigated. The results of hardness tests made at shafts after drawing with 15 or 20 deg followed by CRS process are presented in Figure 7 for several diameter lines. Mean values of hardness were calculated in the surface and core regions (0 to 3, 8 to 12, and 17 to 20 mm). The shafts show varied hardness values (Figure 7), which are generally higher in the surface zones than in the cores. This is due to the work hardening caused by plastic deformation in the drawing and CRS processes. The 20 deg drawn shaft reaches a higher surface hardness than the 15 deg drawn shaft. This means that the drawing angle of 20 deg resulted in higher plastic deformation in the surface zones than that of 15 deg drawing angle. This is in accordance with the deformation zone geometry, that 20 deg has a larger Δ parameter compared with 15 deg. It means a stronger plastic flow in the deformation zone. It is assumed that the influence of the CRS process, which was carried out identically for the two drawing processes, is identical for both. Moreover, the hardness presents variations according to the angular position, indicating inhomogeneous plastic deformation existing around the circumference. This inhomogeneity can be attributed to the varied initial diameters of the wire and the pre-straightening process.

Local strong plastic deformations can be observed in the surface zones by metallographic analyses (Figure 8). The plastically deformed surface regions present variations at different longitudinal lines and along the same line, which confirms the previously observed inhomogeneities. In Figure 8, a stronger local plastic deformation can be observed in the case of the 20 deg drawn sample.

The axial residual stresses at the surface of the shafts after drawing and CRS were determined by XRD for several angle lines at different distances from the shaft end (Figure 9). It can be observed that for both treatments, more or less inhomogeneous surface residual stress distributions are present. The average stress values are -255 ± 10 MPa and -261 ± 16 MPa for the 15 and 20 deg drawn shafts after CRS, respectively. It should be remarked that the CRS influences the RS state of the shafts strongly,[16] while the difference could be traced back to the drawing processes before CRS. The corresponding FWHM values of the diffraction peaks are, respectively, 2.05 $\pm$ 0.03 and 2.11 $\pm$ 0.02 deg, which

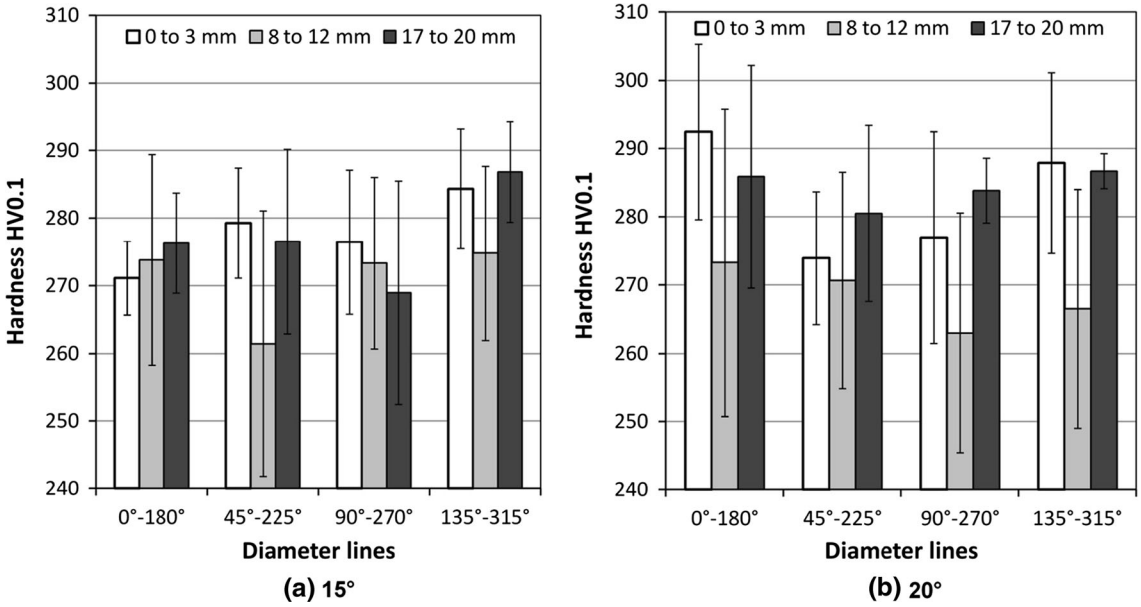

Fig. 7—Average values of hardness in the surface zone and in the core along four diameter lines at the cross section of shafts after (*a*) 15 deg and (*b*) 20 deg drawing (and after CRS).

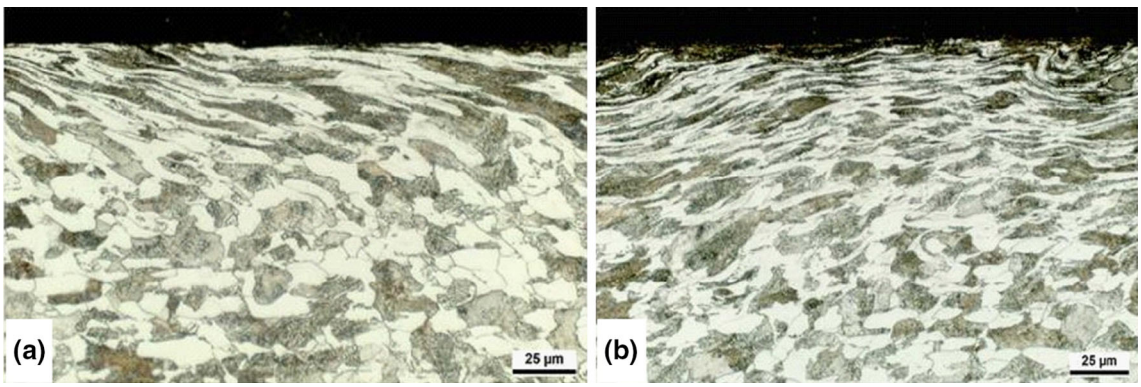

Fig. 8—Local plastic deformation in the microstructure along a peripheral line in the longitudinal section observed by optical microscopy, (*a*) 15 deg drawing and (*b*) 20 deg drawing.

give further information that the work hardening caused by the 20 deg drawing is more pronounced than the 15 deg drawing. For comparison the FWHM values of a pre-straightened shaft before drawing are found in the range from 1.93 to 1.58 deg in the zone from the surface up to a depth of 0.5 mm. The 20 deg drawn shaft in Figure 9(b) presents noticeable larger inhomogeneities in the residual stress distributions in length direction than the 15 deg drawn shaft in Figure 9(a). The residual stresses of the 20 deg drawn shaft at 180 deg vary from −279 MPa at 140 mm (axial position) to −233 MPa at 190 mm (Figure 9(b)), and similar ES variations are also observed at 0 deg with the value of −250 MPa at 140 mm and −290 MPa at 190 mm. Such RS variations extended in the length indicate the presence of a bending distortion potential.

The distribution of the residual stresses in the cross section of the shafts after different process steps was further analyzed by non-destructive neutron diffraction measurements, and the results were published elsewhere.[16] The residual stress state in the cross section was proved to change largely by each process step from pre-straightening, drawing, CRS, and induction hardening.

The residual stress state after shear cut has been analyzed in detail at eight angular positions (45 deg from each other), and 14 axial distances between 2 and 42 mm from the cut end of one shaft. Figure 10 shows only a few curves from the large amount of data, in order to present the results readably. A strong plastic deformation can be observed at the shear cut end of the shafts occurring by the onset of the shear blade (Figure 10(a)). It caused a large S-shaped variation of the axial residual stresses (Figure 10(b)) between −120 and −460 MPa within the distance up to 42 mm from the cut end. These variations are asymmetric around the circumference (Figure 10(c)). The large variation of residual stresses due to shear cutting indicates a local significant distortion potential near the cut end.

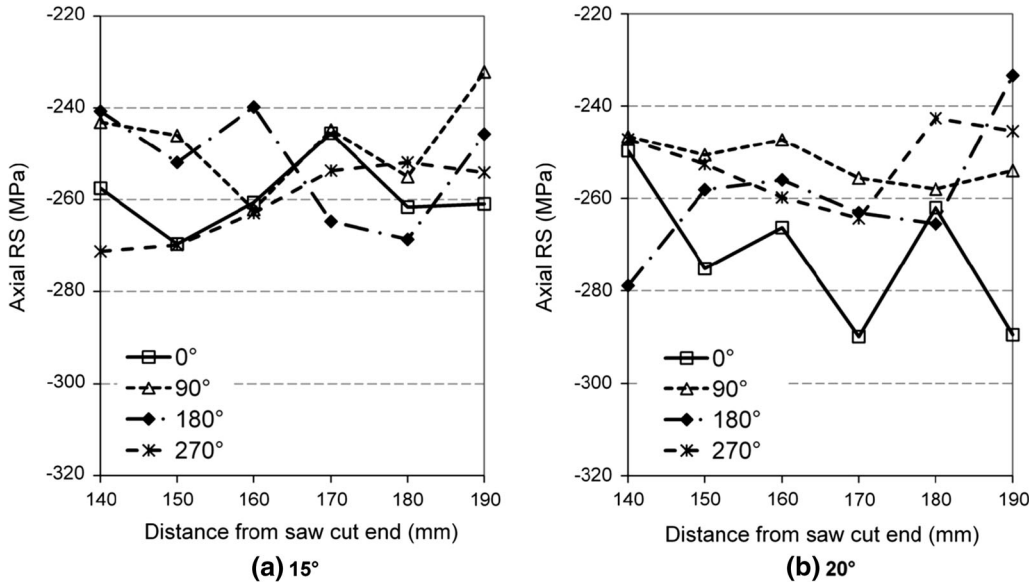

Fig. 9—Axial residual stresses along four angle lines in dependence on the distance (140, …, 190 mm) to the notched (saw cut) end of the shafts, (*a*) 15 deg and (*b*) 20 deg drawing after CRS.

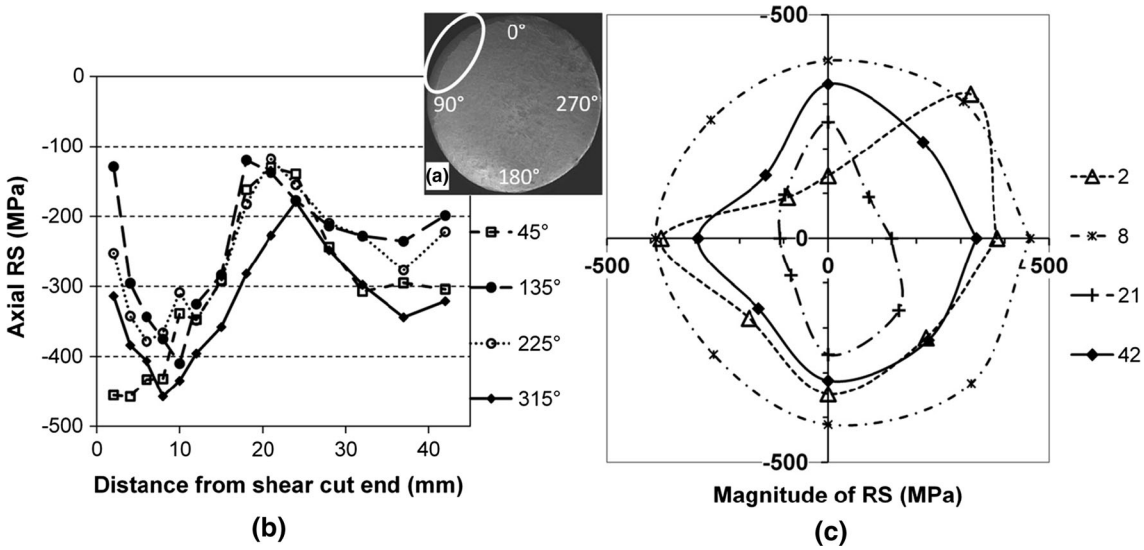

Fig. 10—Scanning electron microscope image of the shear cut surface (*a*), values of axial residual compressive stresses of four angular positions at 14 distances (2, …, 42 mm) from the shear cut end (*b*), and in (*c*) Polar diagram of axial residual compressive stresses of four circles of the shaft (after 20 deg drawing and CRS).

C. *Dimensional Characterization Before Induction Hardening*

The axial curvatures of the shafts (in 108 samples) after drawing, CRS, and cutting (before induction hardening) determined by 3D measurements showed similar distribution for both drawing processes presenting an average curvature of 20 ± 12 μm for the 20 deg drawing and 20 ± 11 μm for the 15 deg drawing, respectively (Figure 11). Therefore, no significant difference regarding the influence of drawing processes as well as cuttings on the distortion before induction hardening can be observed.

Figure 12 illustrates the result of 3D co-ordinate measurements of one shaft after 15 deg drawing and CRS. The central positions of the measured circles (see Figure 4) are projected on R–Z plane (Figure 12(a)) and on the X–Y plane (Figure 12(b)). The curvature vector of the shaft was calculated to be 50 μm at the angular position of 228.5 deg from the central points of the circles with 20 mm diameter. This represents the shape alteration of the shaft (considered length, $L2$ = 366 mm) from of the ideal straight cylinder. The central positions of the three circles at each notch (see Figure 4), with the diameter of 16 and 18 mm, appear

deviated from the central axis. As mentioned above, the two notches were machined in all shafts before drilling the central holes at the ends of the shafts. This machining procedure led to eccentricity of the notches from the central axis of the shafts.

D. *Microstructure and Hardness After Induction Hardening*

The induction heat treatments were conducted to achieve either a SHD of 1.2 or of 2.2 mm by varying the heating power, which resulted in the austenitizing temperature of 1123 K or 1243 K (850 °C or 970 °C), respectively. The hardened surface layers (cases) of the notched and un-notched segments (with the diameters of 16, 18, and 20 mm) of two shafts are presented in Figure 13 appearing as dark-etched surface zones in the optical micrographs. The non-transformed core and the transition layer between the case and the core can also be distinguished. Additionally, the core segregations (appearing as dark region near the center) with varying positions and more (Figures 13(a) through (c) or less (Figures 13(d) through (f)) pronounced aspect were observed. The core segregations varied in their intensities, patterns, and positions within a single shaft and from a shaft to another for the same drawing process. It indicates that the local chemical composition and the segregations are inhomogeneous in the same material batch.

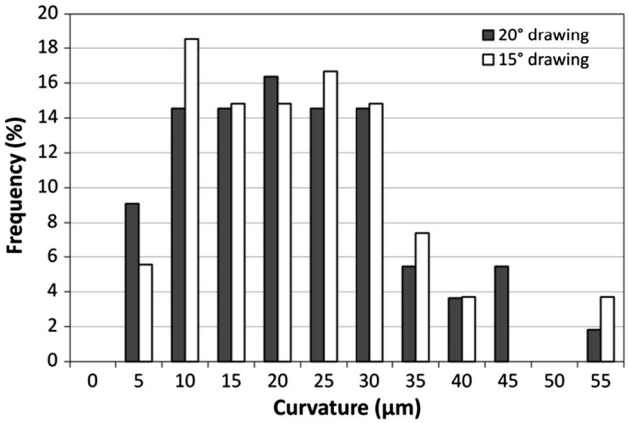

Fig. 11—Distribution of the curvatures of the shafts after drawing and CRS related to the drawing processes with 20 and 15 deg drawing angle (evaluated length $L2 = 366$ mm).

In detail, the case layers have martensitic microstructures (Figure 14). The martensite needles in the surface layers of the shaft with SHD 1.2 mm (Figure 14(a)) are finer than those with SHD 2.2 mm (Figure 14(b)). This can be attributed to the different austenitizing temperatures. The higher austenitizing temperature has been reached for higher case depths by increased heating power. The transition layers are characterized by microstructures composed of martensite and ferrite. It should be remarked, that the coarse martensite needles in the surface layer of the shaft with SHD 2.2 mm are not ideal, since the mechanical properties of the steel might be lowered.[17,18]

Figure 15 shows the hardness profiles and the determined SHD values of the two shafts presented in Figure 13 at the three segments, with the diameters of 16 mm (D16), 18 mm (D18), and 20 mm (D20), for both induction hardening processes. The target SHD values are reached, and the deviations are small and acceptable. The ranges between 600 HV1 and 270 HV1 (core hardness) on the hardness profiles illustrate the transition layers, which were influenced by SHD, notches, and parameters of the induction hardening.

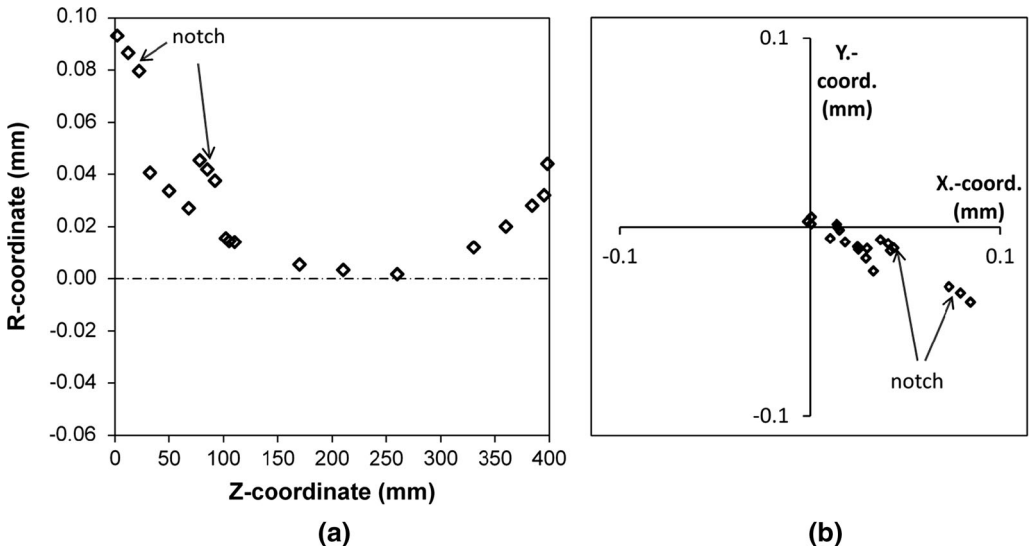

Fig. 12—Central positions of the measured circles (see Fig. 4) on *R–Z* plane (*a*) and in (*b*) on the X–Y plane; the curvature vector (50 μm, 228.5 deg) of the shaft was calculated from the points of 20 mm circles (15 deg drawing and CRS; the deviated points correspond to the two notches).

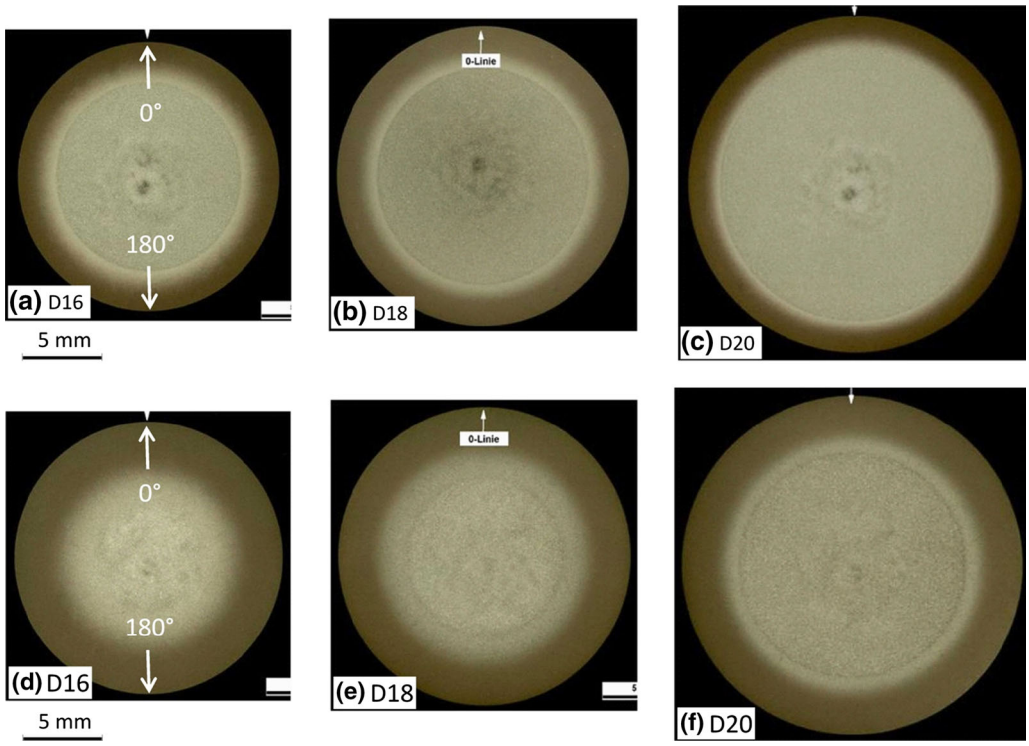

Fig. 13—Macrostructures at the cross sections of two shafts (15 deg drawing, CRS) after induction hardening with SHD 1.2 mm (*a*) through (*c*) and 2.2 mm (*d*) through (*f*), respectively, (tempered 2 h at 443 K (170 °C)).

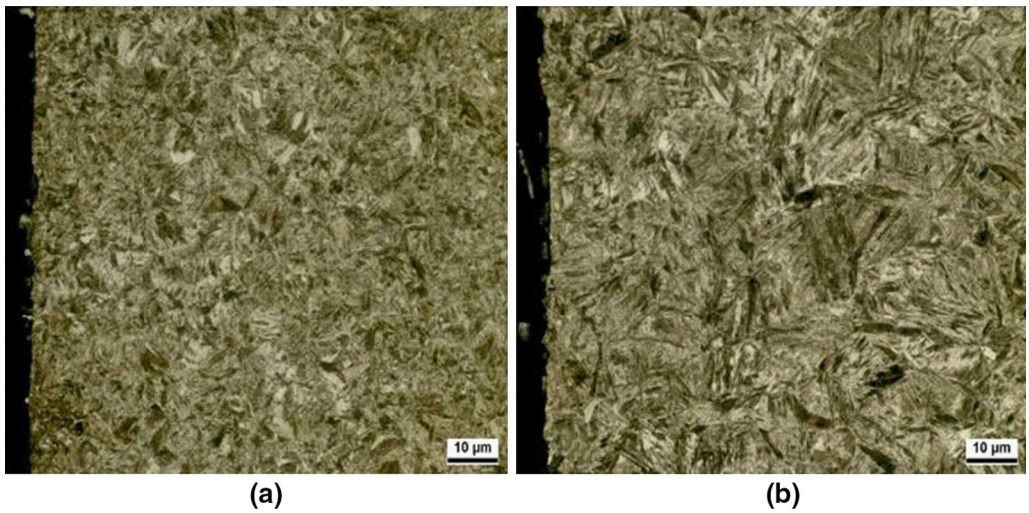

Fig. 14—Microstructures of the hardened surface layers of the shafts (*a*) in Fig. 13(c), and (*b*) in Fig. 13(f).

E. *Dimensional Characterization After Induction Hardening*

The size alterations of the shafts after induction hardening are given in Table III. A diameter increase takes place, which is more pronounced with increasing SHD. In the same time, the sample lengths decreases and the amount of the changes decreases with increasing SHD. This kind of size alterations is observed similarly in the shafts of both drawing variations. The mean volume changes of the shafts are about 0.067 pct for SHD 1.2 mm and ca. 0.114 pct for SHD 2.2 mm. These volume changes are essentially due to the martensitic transformed surface layer and due to the higher specific volume of martensite compared to ferrite and pearlite. The anisotropic nature of size alterations can be attributed to the influence of thermal and transformation stresses during the heat treatment.[19]

The curvatures of 80 samples after the induction hardening show large increase in the magnitude compared with those before hardening (Table IV). The

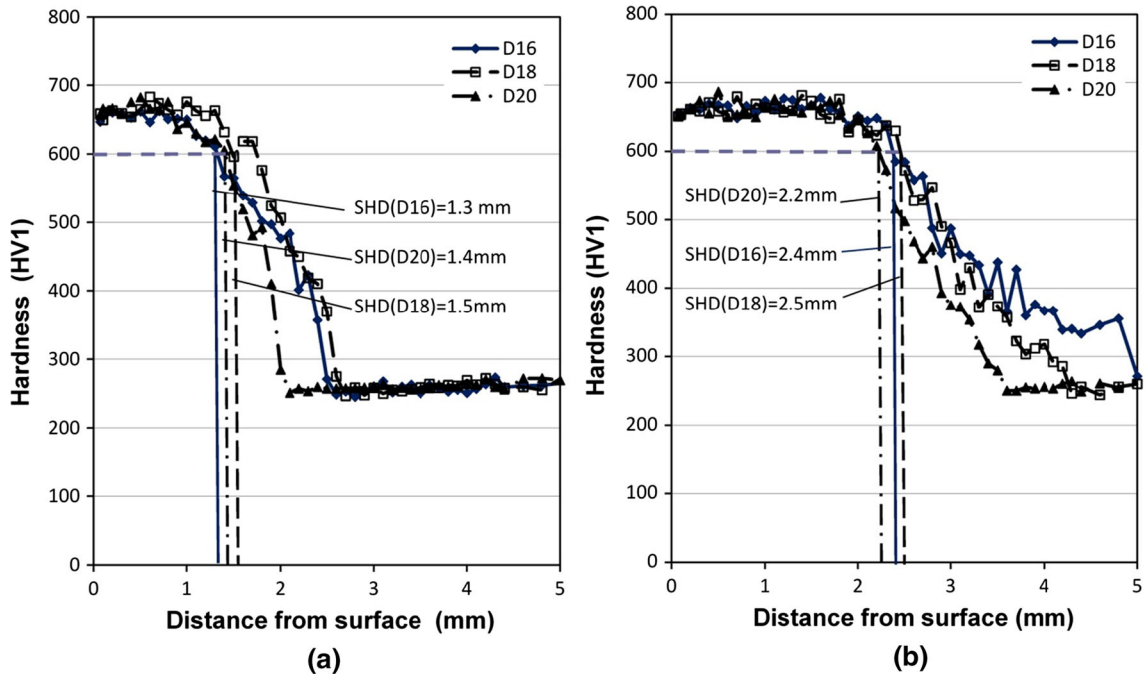

Fig. 15—Hardness profiles and determined SHD values of the shafts presented in Fig. 13 after induction hardening processes with the target SHD values of (*a*) 1.2 mm and (*b*) 2.2 mm, respectively, (tempered 2 h at 443 K (170 °C)).

Table III. Diameter and Length Change of the Shafts Induced by the Induction Hardening Processes

	Dimensional Change (pct)	
Condition	Diameter	Length
20 deg-SHD1.2	0.046	−0.029
20 deg-SHD2.2	0.066	−0.010
15 deg-SHD1.2	0.051	−0.031
15 deg-SHD2.2	0.062	−0.018

Table IV. Curvatures of the Shafts Before and After the Induction Hardening Processes

	Curvature (μm)	
Condition	Before IH	After IH
20 deg-SHD1.2	23 ± 12	66 ± 28
20 deg-SHD2.2	23 ± 12	96 ± 47
15 deg-SHD1.2	19 ± 10	184 ± 54
15 deg-SHD2.2	25 ± 13	193 ± 63

mean curvatures of the variation 20 deg drawing with SHD 1.2 mm and SHD 2.2 mm are determined to be 66 ± 28 and 96 ± 47 μm, respectively, while values of 184 ± 54 and 193 ± 63 μm were determined for the variation 15 deg drawing with each SHD 1.2 mm and SHD 2.2 mm. Additionally, the curvature vectors of the 15 deg drawn samples are preferably orientated in directions between 90 and 180 deg, while for the shafts drawn with 20 deg tool the vectors are nearly statistically distributed (Figure 16). The evaluation in Figure 16 used the length $L3 = 296$ mm in order to exclude the influence of the notch ($D2 = 18$ mm) on the curvature directions. These results show that significant shape distortion occurred to the 15 deg drawn shafts with preferred orientation, although these could not be observed before the induction hardening.

From these results it is still not clear, if the drawing angle itself is the reason of the different distortion behaviors, regarding the fact that the drawing process involves further parameters, *e.g.*, die alignment, lubrication *etc.* beside the drawing angle. For example, misalignment of the drawing die could be a possible reason, as reported by Haenisch *et al.*[20] derived from a finite element analysis (FEA). The simulation result indicated that if the drawing die has one degree misalignment of the central axis, large asymmetric RS distribution in the shaft can be induced during drawing. The asymmetric distributed RS could then cause a bending distortion.[5,20] However, in the current experiments, a clear correlation between the distortion after induction hardening and the inhomogeneous residual stresses in the 15 deg drawn shifts before induction hardening could not be found. A possible explanation, therefore, could be the limited number of samples for the analysis of residual stresses, because only one sample was selected randomly from each batch of drawn shafts for the RS analysis and this sample might not be representative for the whole batch of the shafts. Additionally, the RS measurements were done after CRS at the surface, where the largest changes of RS normally occur, but the RS in the entire cross section should be considered in distortion potentials.

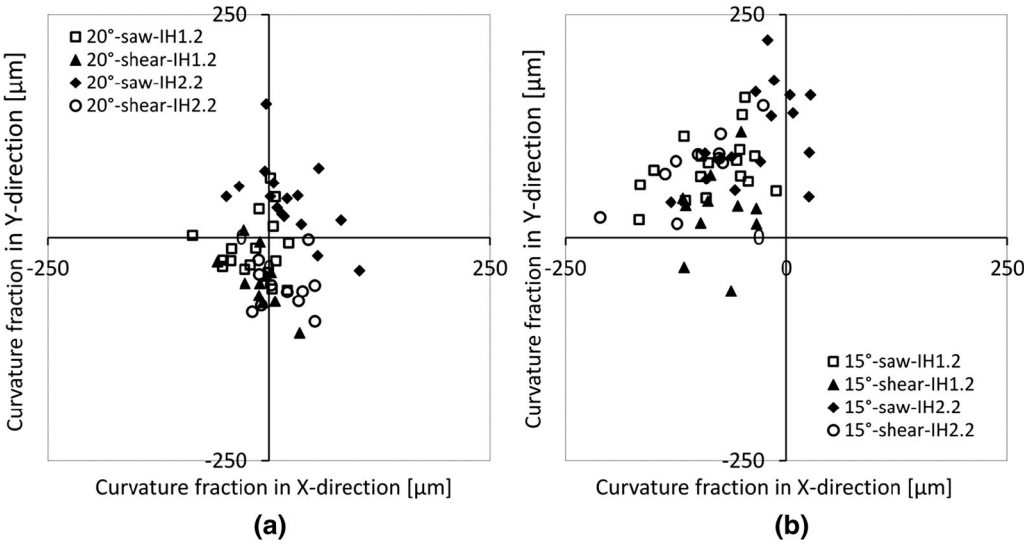

Fig. 16—Curvature vectors of (*a*) 20 deg and (*b*) 15 deg drawn shafts after induction hardening with SHD 1.2 mm and SHD 2.2 mm, respectively, (tempered 2 h at 443 K (170 °C); evaluated length $L3 = 296$ mm).

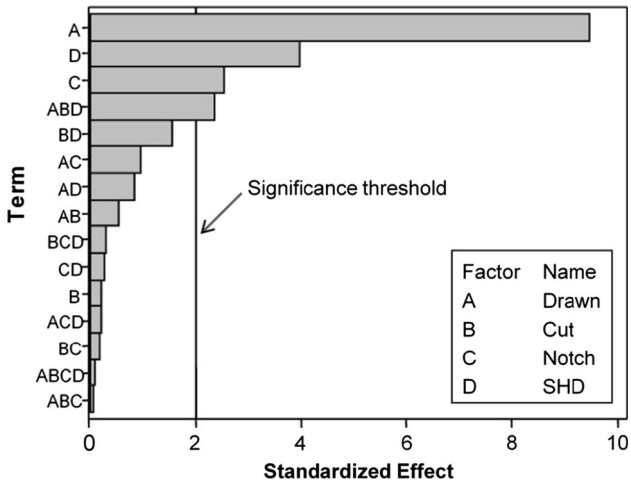

Fig. 17—Pareto chart of the statistical analysis of the curvatures of the hardened shafts (error rate $\alpha = 0.05$). The factors with standardized effect larger than two are significant.

F. *Statistic Evaluation of DoE*

The statistic analysis of the full factorial DoE plan with 2^4 runs regarding the curvature of the shafts after induction hardening achieved a result with a 95 pct confidence level (Figure 17). It indicates that the drawing process is the most significant distortion factor, while the SHD of the induction hardening plays a still significant but secondary role. The significance of the shaft geometry (notches) takes the third place, followed by the interaction of the drawing, cutting, and induction hardening. This result demonstrated that the relevant factors affecting distortion in a manufacturing process chain could be identified with the help of the statistic analysis of DoE.

IV. CONCLUSION

Effects and correlations between process parameters and distortion occurring along a process chain for the production of hardened steel shafts were investigated by Design of Experiments (DoE). Four essential process parameters as "influencing factors" in the manufacturing process chain regarding cold drawing, saw or shear cutting, notches on the shafts, and inductive hardening were involved in the DoE plan. The results of the statistical analysis of the DoE showed that the drawing process is the most important distortion factor. The surface hardening depth (SHD) of induction hardening is the second main factor. The shaft geometry (notches) takes the third place, followed by the interaction of the drawing, cutting method, and induction hardening. The results confirmed the finding in previous studies[21,22] and in agreement with other research works[5,20,23] regarding distortion of cold-formed components.

In detail, the curvatures of the shafts before the hardening lay in the range up to 50 micrometer and these increased up to 200 micrometer after the induction hardening. In particular, the 15 deg drawing process combined with the induction hardening with SHD 2.2 mm led to the largest distortion. Moreover, the curvature vectors of the 15 deg drawn shafts orientated in preferred directions, which were absent before the induction hardening. Although several inhomogeneities, such as local chemical composition, local plastic deformation as well as local residual stress state were found in the work pieces before the hardening, a clear correlation between the inhomogeneities, particularly inhomogeneous residual stresses, in the work pieces before induction hardening and the distortion afterward could, however, not be found.

Nevertheless, it could be shown that by the selection of suitable process parameters (in this case, mainly the cold drawing process with suitable parameters and a small SHD

of induction hardening) the distortion could be reduced by at least about 66 pct. This can benefit industrial production for lowering the cost of the final grinding largely.

Further research works including numerical simulation of the different manufacturing processes are ongoing for clarifying the relationship between the residual stress states of the shafts after drawing, after CRS straightening, and distortions after induction hardening.

ACKNOWLEDGMENTS

This work was done in the frame of the "BRAG-ECRIM" program (Brazilian German Cooperation Research Initiative in Manufacturing). The authors are deeply indebted to DFG, CAPES, and CNPq for financial support. This research also has been supported by the European Commission under the 7th Framework Program through the Key Action: Strengthening the European Research Area, Research Infrastructures: Contract No. 226507 (NIMI3).

REFERENCES

1. F. Hoffmann, O. Keßler, T. Luebben, and P. Mayr: *Heat Treatm. Metals*, 2004, vol. 29 (8), pp. 61–66.
2. O. Keßler, C. Prinz, T. Sackmann, L. Nowag, H. Surm, F. Frerichs, T. Luebben, and H.W. Zoch: *Materialwiss. Werkstofftech.*, 2006, vol. 37, pp. 11–18, DOI:10.1002/mawe.200500975.
3. Z. Wang and B. Gong: *ASM Handbook of Residual Stress and Deformation of Steel*, ASM International, USA, 2002, pp. 141–149.
4. K.D. Thoben, T. Luebben, B. Clausen, C. Prinz, and A. Schulz: *Proc. 4th Int. Conf. Quenching and Control of Distortion*, Beijing, China, 20–23 May 2003, pp. 325–31, http://search.proquest.com/docview/27850729?accountid=14136.
5. N.B. Khalifa: *Report of the Research IGF 309ZN*, Dortmund, Germany, 2012.
6. H.W. Zoch: *Materialwiss. Werkstofftech.*, 2005, vol. 2006 (37), pp. 6–10, DOI:10.1002/mawe.200500958.
7. H.W. Zoch and T. Luebben: *Proc. 6th Int. Quenching and Control of Distortion Conf.*, Chicago, USA, 2012, pp. 1–11.
8. K. Siebertz, D. van Bebber, and T. Hochkirchen: *Statistische Versuchsplanung—Design of Experiments (DoE)*, Springer, Berlin, 2010. e-ISBN 978-3-642-05493-8, DOI:10.1007/978-3-642-05493-8.
9. W. Kleppmann: *Taschenbuch Versuchsplanung*, Carl Hanser, Munich, Vienna, 2001.
10. H. Surm, O. Kessler, F. Hoffmann, and P. Mayr: *Int. J. Mater. Prod. Technol.*, 2005, vol. 24, pp. 270–81, DOI:10.1504/IJMPT.2005.007954.
11. F. Frerichs, Th. Luebben, F. Hoffmann, and P. Mayr: *Int. J. Mater. Prod. Technol.*, 2005, vol. 24 (1–4), pp. 244–58, DOI:10.1504/IJMPT.2005.007952.
12. I.C. Noyan and J.B. Cohen: *Residual Stress, Measurement by Diffraction and Interpretation*, Springer, New York, 1987.
13. J. Epp and T. Hirsch: *Materialwiss. Werkstofftech.*, 2011, vol. 2012 (43), pp. 112–19, DOI:10.1002/mawe.201100897.
14. M.L. Martinez-Peres, F.J. Mompean, J. Ruiz-Hervias, C.R. Borlado, J.M. Atenzia, M. Garcia-Hernandez, M. Elices, J. Gil-Sevillano, R.L. Peng, and T. Buslaps: *Acta Mater.*, 2004, vol. 52, pp. 5303–13.
15. K. van Acker, J. Root, P. van Houte, and E. Aernoudt: *Acta Mater.*, 1996, vol. 10, pp. 4039–44.
16. J. Dong, J. Epp, A. Rocha, R.M. Nunes, R. Wimpory, and H.W. Zoch: *HTM J. Heat Treat. Mater.*, 2014, vol. 69, pp. 348–359, DOI:10.3139/105.110244.
17. R.A. Grange: *ASM Trans. Quert.*, 1966, vol. 59 (1), pp. 26–48.
18. G. Krauss: *Mater. Sci. Eng.*, 1999, vols. A273–275, pp. 40–57.
19. H. Fahry, H.-W. Zoch, and H. Schlicht: *HTM Haerterei-Tech. Mitt.*, 1989, vol. 44, pp. 149–56.
20. S. Haenisch, S. Ossenkemper, A. Jaeger, N.B. Khalifa, A.E. Tekkaya, D. Nadolski, A. Schulz, F. Hoffmann, and H.W. Zoch: *Proceedings of the 45th ICFG Plenary Meeting*, Nagoya, Japan, 9–12 September 2012, pp. 32–38.
21. A.S. Rocha, R.M. Nunes, T.F. Souza, C.A.T. Soares, A. E. Tekkaya, and T. Hirsch: *HTM, J. Heat Treat. Mater.*, 2013, vol. 68, pp. 135–141, DOI:10.3139/105.110187.
22. T. Hirsch, A.S. Rocha, and R.M. Nunes: *Metall. Mater. Trans. A*, 2013, vol. 44A, pp. 5806–16, DOI:10.1007/s11661-013-1952-z.
23. D. Nadolski, S. Haenisch, A. Schulz, N.B. Khalifa, F. Hoffmann, H.W. Zoch, and A.E. Tekkaya: *3rd Int. Conf. Distortion Engineering, 2011*, Bremen, Germany, 14–16 September, 2011, pp. 267–274.